Secondary reverse streamer observed in an ester insulating liquid under negative impulse voltage

2011 J. Phys. D: Appl. Phys. 44 405203

(http://iopscience.iop.org/0022-3727/44/40/405203)

IOP Publishing Journal of Physics D: Applied Physics
J. Phys. D: Appl. Phys. **44** (2011) 405203 (9pp) doi:10.1088/0022-3727/44/40/405203

Secondary reverse streamer observed in an ester insulating liquid under negative impulse voltage

Q Liu and Z D Wang

School of Electrical and Electronic Engineering, The University of Manchester, Sackville Street, Manchester M13 9PL, UK

E-mail: zhongdong.wang@manchester.ac.uk

Received 18 June 2011, in final form 18 August 2011
Published 15 September 2011
Online at stacks.iop.org/JPhysD/44/405203

Abstract
The so-called 'secondary reverse streamer (SRS)' in this study depicts a newly observed streamer-in-liquid phenomenon which subsequently occurs well after the extinction of the primary streamer (PS) propagation within a single shot of negative impulse voltage and has reverse polarity to the PS. Tests were carried out in a synthetic ester liquid at a 50 mm needle–plane gap under negative impulse voltages up to 140 kV. Based on the current and light waveforms as well as the photographic images, two types of SRS were found: one has a bright trunk with a high velocity of 9.79 km s^{-1} belonging to the 3rd mode streamer; and the other has a weak tree-like channel with a low velocity of 1.28 km s^{-1} resembling the 2nd mode streamer. It should be emphasized that SRS under negative impulse voltages has positive polarity being opposite to the negative PS, which is believed to be due to the reverse electric field induced by the residual space charges left by the PS. This has been confirmed by further verification tests under tail-chopped impulse voltages, for SRSs are significantly enhanced in both axial and lateral directions after the early removal of the external applied field.

(Some figures in this article are in colour only in the electronic version)

1. Introduction

Insulating liquids have been widely used in high-voltage power equipment, e.g. transformers and cables, for many decades. Ester liquids with their merits of good biodegradability and low fire risk are being considered as alternatives to the traditional sources, e.g. mineral oil. Wide applications of these new liquids can be expected; however, it takes time for industry adoption and thus requires a thorough understanding of esters' dielectric properties, particularly on discharge behaviours and breakdown performances.

The discharge events during the pre-breakdown stage in liquids are commonly called streamers. However, a streamer in liquids is different from a streamer in gases, which normally propagates in a continuous manner with minimum velocities of 10–100 km s^{-1} [1]. In general, four modes of streamers in liquids were recognized based mainly on the average propagation velocity, namely 1st, 2nd, 3rd and 4th mode with typical velocities of 0.1 km s^{-1}, 1–2 km s^{-1}, 10 km s^{-1} and 100 km s^{-1}, respectively [2, 3]. The higher the applied electric field, the higher will be the mode of the streamer observed.

Since initiation of a streamer in liquids requires a strong electric field (a few MV cm^{-1}) [4], needle–plane electrodes are widely used to generate a streamer. An extensive effort was made in the past decades to explore the streamer characteristics in liquids under various test conditions [3, 5–12], and a number of review papers [3, 5, 13, 14] have been produced to summarize the streamer phenomena in liquids; however, a universally agreed conclusion has not yet been achieved.

In the field of surface discharge, phenomenon of back discharge, having opposite polarity to the applied voltage, has been observed on solid surfaces under both positive and negative impulse voltages. The solid surface was sandwiched between the needle and plate electrodes and exposed to air environment [15, 16]. During the falling (or ending) period of impulse voltage, the needle electrode exhibited opposite polarity with respect to the previously charged surface. If the reverse electric field induced by the surface charge was

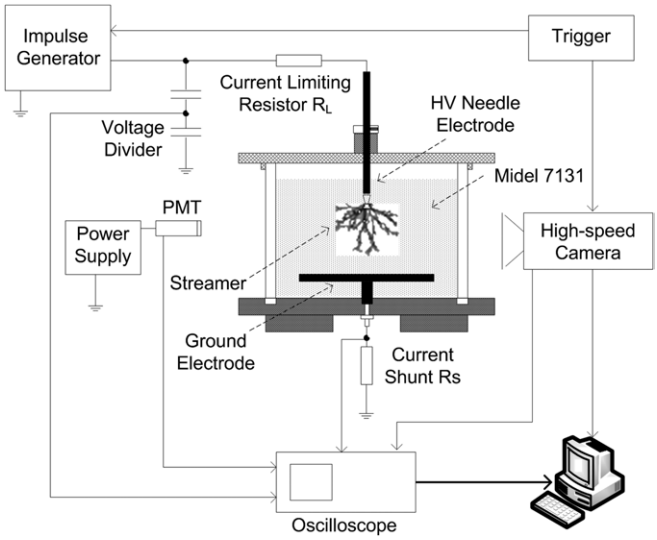

Figure 1. Sketch of the experimental setup.

strong enough, back discharge could be observed. A similar phenomenon was also reported on a solid surface immersed in mineral oil under lightning impulse voltage [17]. A 'secondary' back discharge occurred approximately 100 μs after the main discharge evidenced by the current waveform. It is well known that back discharges on solid surface take advantage of the charge memory effect of solid dielectrics, which helps trapping the residual space charges on the surface thus further leading to the reverse electric field. Therefore, it is not expected to observe such a phenomenon in open liquid gaps, i.e. without the presence of a solid surface.

This paper, however, depicts a newly observed streamer-in-liquid phenomenon which occurs subsequently and well after the extinction of the primary streamer (PS) propagation within a single shot of negative impulse voltage and has reverse polarity to the PS as well as to the applied impulse voltage. This phenomenon is similar to the back discharge phenomenon on a solid surface. However 'streamer' is commonly used to describe a discharge phenomenon in liquids, and its occurrence is secondary and the polarity is in reverse to the PS, so we arbitrarily name this newly observed phenomenon 'secondary reverse streamer (SRS)' in this paper. The tests were carried out in a 50 mm needle–plane gap under negative impulse voltages up to 140 kV. Characteristics of SRS including length, velocity, light intensity and time of occurrence were described. In addition, the mechanism of SRS was discussed. Finally, tests under tail-chopped impulse voltages were used to verify the mechanism interpretation.

2. Experimental description

The experimental setup is shown in figure 1. A cubic-like test cell with a volume of 12.5 L was used to hold the liquid sample and needle–plane electrodes. Side walls and top lid of the test cell were made of transparent Perspex material, which facilitated streamer observation. A tungsten needle was used whose tip radius of curvature was guaranteed to be 50 ± 5 μm after selection using a microscope. The plane electrode was made of brass, having a diameter of 200 mm and edge radius of 3 mm. The needle–plane gap was fixed at 50 mm.

An impulse generator with a maximum voltage of 2000 kV was used to deliver the standard lightning impulse with 1.2 μs front time and 50 μs half tail time. A small current limit resistor (3.5 kΩ) was used to protect the liquid sample and needle electrode in case a breakdown occurred. Voltage and current waveforms were recorded using a high-voltage capacitive divider and a non-inductive current shunt (1 Ω), respectively.

A high-speed camera, which consisted of 16 high-resolution intensified CCD sensors interfaced with a beam splitter, was used to take the integral light image (still image) of streamers. Each image can be individually set to a different exposure time from 5 ns to 10 ms in steps of 5 ns. The interframe time between images can also be independently set from 0 ns to 20 ms in steps of 5 ns. In this study, frame 1 was used to record the PS. The subsequent 15 frames with the same fixed exposure time were regularly spread out to capture the SRS. The interframe time was set as 0 μs to avoid missing information during the observation. Meanwhile, a compact photomultiplier tube (PMT) within a shielding box was used to record the light intensity.

A manual trigger unit was used to trigger the impulse generator and high-speed camera to ensure that voltage, current and light signals were recorded in a synchronized manner with the camera. Approximately 5 min resting time was given between two consecutive tests (one shot per test). According to previous experience, there would not be an accumulative effect expected which means a single test is independent of another.

The liquid under investigation is a type of synthetic ester, Midel-7131, of which the PS characteristics have been reported in [18]. It is a halogen-free pentaerythritol ester, which contains '–COOR' groups in the molecule. The high electronegative performance of oxygen atom in '–COOR' group makes the synthetic ester Midel-7131 slightly polar. The relative permittivity is therefore higher and the volume resistivity is lower than that of normal hydrocarbon-based insulating liquids, e.g. mineral oil.

Testing samples were directly taken from sealed new oil barrels. The relative humidity of testing liquids was regularly checked during the whole period of experiments, which scattered in the range from approximately 5% to 20% RH. All the experiments were carried out in a small dark room at ambient temperature and atmosphere pressure.

3. Results and discussion

3.1. Phenomenon of SRS

Two types of SRS were observed under negative impulse voltages as shown in figures 2 and 3, respectively.

Figure 2 demonstrates a type-A secondary reverse streamer (SRS-A) obtained at 120 kV. Figure 2(*a*) presents a global scenario of the PS and SRS. A cluster of intense current and light pulses was recorded after the onset of applied impulse voltage spreading from the beginning to the end of

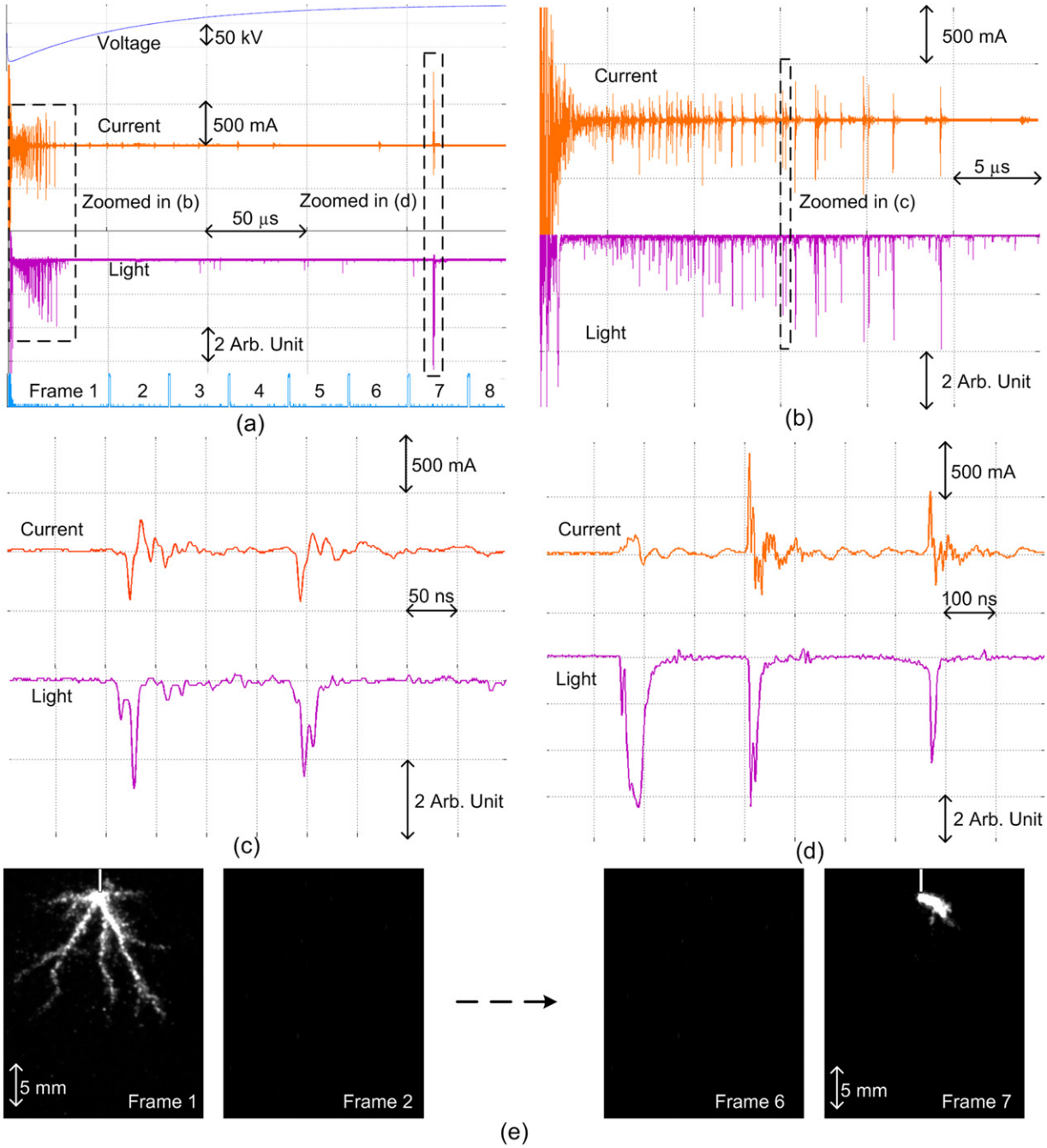

Figure 2. Demonstration of SRS-A ($d = 50$ mm, $V = 120$ kV), (a) global scenario, (b) propagation of PS, (c) polarity of PS, (d) polarity of SRS, (e) streamer images, 50 μs exposure time for frame 1 and 30 μs exposure time for frames 2–8.

the PS. This is the complete PS process which is normally the focus of pre-breakdown study. However, we observed an SRS with large magnitude short duration current and light signals, which occurred 184.2 μs after the extinction of the PS. It is noteworthy that the impulse voltage decayed to approximately 5 kV when the SRS appeared.

The zoomed-in current and light signals of the PS are shown in figure 2(b), of which each is composed of a train of irregularly spaced discrete pulses. The charging process induces some noises in both current and light signals at the rising period of the impulse voltage, and these noises are consequently ignored in the following analysis. Throughout the streamer propagation, the current and light pulses increase in amplitude gradually with time. Most of the light pulses can be correlated with the current pulses in terms of occurrence time, which depict the full re-illumination from the needle tip to the head of the streamer [19–21]. Those light pulses which cannot be correlated with the current pulses indicate partial re-illumination that might only exist close to the streamer head [19].

A couple of pulses are further zoomed and shown in figure 2(c) to indicate the polarity of the PS. As light signals measured by PMT are always unidirectional (negative pulses), the polarity of a streamer is determined by the current signal.

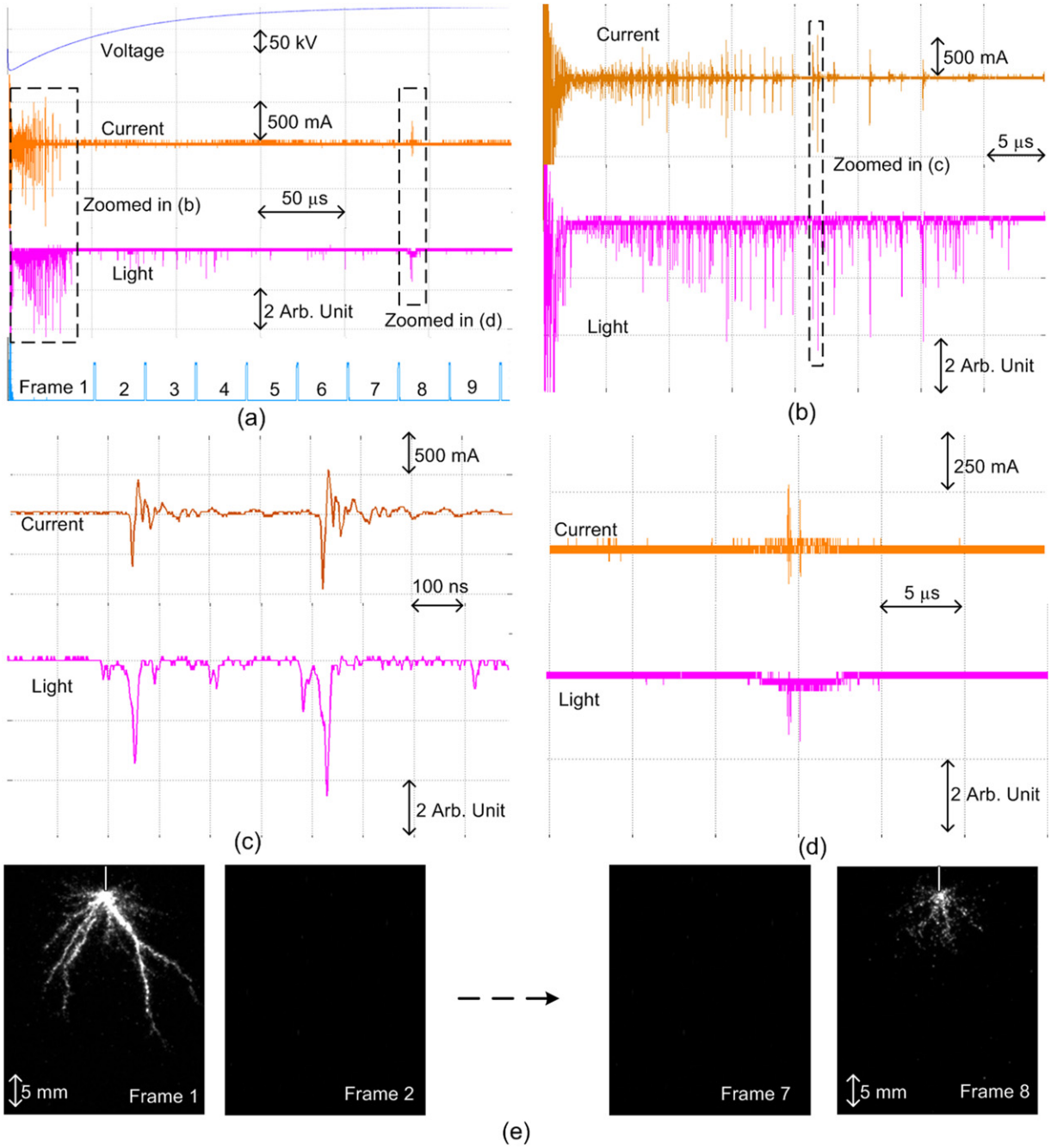

Figure 3. Demonstration of SRS-B ($d = 50$ mm, $V = 140$ kV), (*a*) global scenario, (*b*) propagation of PS, (*c*) polarity of PS, (*d*) polarity of SRS, (*e*) streamer images, 50 μs exposure time for frame 1 and 30 μs exposure time for frames 2–9.

Negative current pulses are observed as expected for the negative PS, which conforms to the customary understanding. So it is surprising to see that the SRS-A is with positive polarity, as shown in figure 2(*d*). In addition, the maximum light intensity of the SRS-A is 6.56 arb. unit, which is about 1.6 times of that of the PS, 4.03 arb. unit. In terms of propagation time as indicated by the current/light signals, it is 26.79 μs for the PS and 0.72 μs for the SRS-A.

Figure 2(*e*) shows the still images. Frame 1 corresponds to the PS while frame 7 corresponds to the SRS-A. There is no other streamer image observed in the interval between PS and SRS-A. The PS appears in a tree-like shape with many branches propagating in both paraxial and lateral directions, and the final stopping length is 17.71 mm. The average velocity of the PS is calculated as 0.66 km s^{-1} using the stopping length divided by the propagation time, and it is regarded as a 2nd mode streamer. The SRS-A image shows a different feature from that of the PS, with a bright single trunk which is 6.76 mm long. It is assumed that the SRS resembles the PS having a propagation process initiating from the needle tip. Therefore the average velocity of the SRS-A is deduced using the same method as 9.36 km s^{-1}, which is over 10 times higher than that of the PS, so it is classified as a 3rd mode streamer.

Figure 3 shows a type-B secondary reverse streamer (SRS-B) observed at 140 kV, which occurred 199.15 μs after the termination of the PS and was with positive polarity. As

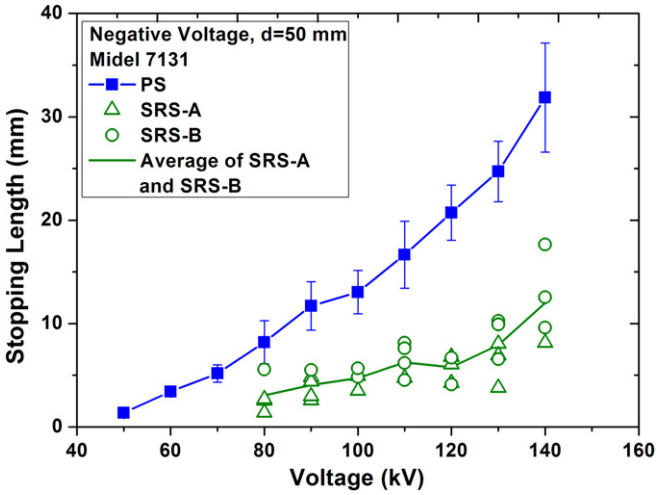

Figure 4. Stopping length of SRS.

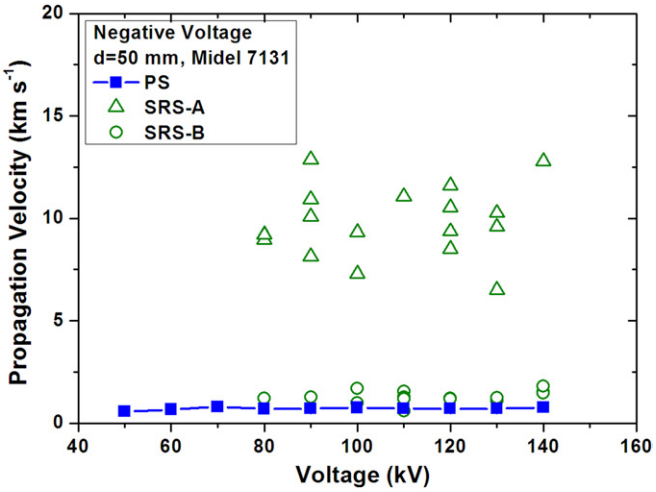

Figure 6. Propagation velocity of SRS.

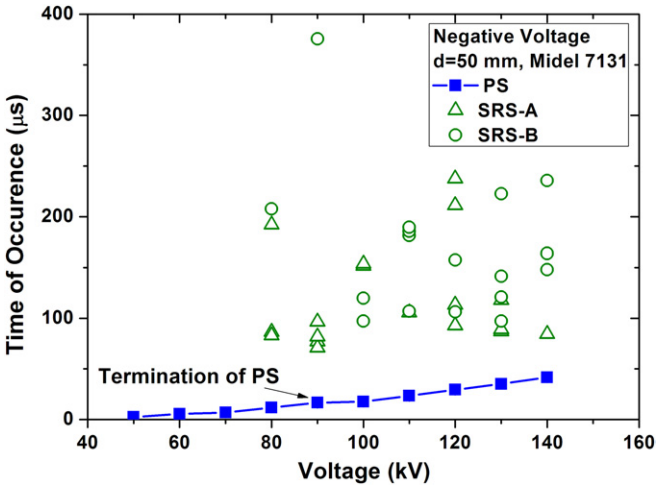

Figure 5. Time of occurrence of SRS.

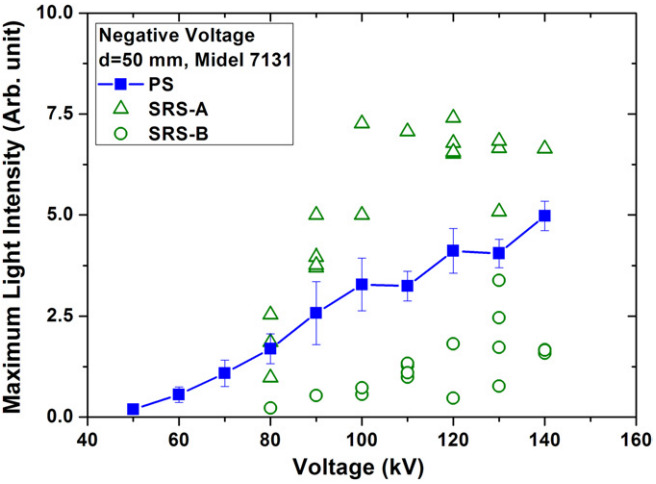

Figure 7. Maximum light intensity of SRS.

shown in figures 3(*b*) and (*c*), the PS has similar features to those observed in figure 2, but the current and light waveforms of the SRS-B, as shown in figures 3(*a*) and (*d*), are quite different from the SRS-A, i.e. for the SRS-B the current and light signals have a continuous component imposed by a few pulses and lasting for more than 5 μs. The maximum light intensity of the SRS-B is 1.66 arb. unit, which is less than half of that of the PS, 4.62 arb. unit. The streamer images in figure 3(*e*) show that the SRS-B has the same tree-like shape as the PS but is weaker in light intensity than the PS. The stopping length and propagation time of the SRS-B are 9.60 mm and 5.33 μs respectively, thus the average velocity of the SRS-B is calculated as 1.80 km s^{-1}, which is the typical velocity for a 2nd mode positive streamer.

3.2. Characteristics of SRS

Figures 4 and 5 show the similarities between SRS-A and SRS-B in terms of stopping length and time of occurrence, respectively, at various voltage levels up to 140 kV. In figure 4, the apparent inception voltage of SRSs is determined as 80 kV, which is 30 kV higher than that of PSs. The lengths of SRSs are shorter than those of PSs, and both increase with an increase in the applied voltage. This somewhat indicates that the inception and strength of SRS are associated with the strength of the corresponding PS. The maximum length of SRSs is 17.65 mm observed at 140 kV, which is about half of the corresponding PS. In figure 5, time of occurrence of SRSs seems uninfluenced by the applied voltage levels, i.e. neither a monographically upward nor downward trend is observed. The mean time of occurrence for all the SRSs is 142.57 μs, at which the impulse voltage has decayed, on average, to approximately 12% of its peak values.

Figures 6 and 7 show the differences between SRS-A and SRS-B in terms of average propagation velocity and maximum light intensity, respectively, at various voltage levels up to 140 kV. In figure 6, the average propagation velocities of PSs are very stable with a mean value of 0.71 km s^{-1}, so are the SRS-Bs with a mean value of 1.28 km s^{-1}. However, the average velocities of SRS-As are much higher, with a mean value of 9.79 km s^{-1}. In figure 7, the maximum light intensity of PSs grows gradually with increased voltage. For SRS, the light intensity of SRS-B is lower than that of the PS while that of SRS-A is higher than that of the PS, which conforms to the

Table 1. Characteristics of PS and SRS.

Type	Polarity	Length	Velocity	Light	Shape	Mode
PS	Negative	Long	Low	Normal	Tree-like	2nd
SRS-A	Positive	Short	High	Bright	Trunk	3rd
SRS-B	Positive	Short	Low	Weak	Tree-like	2nd

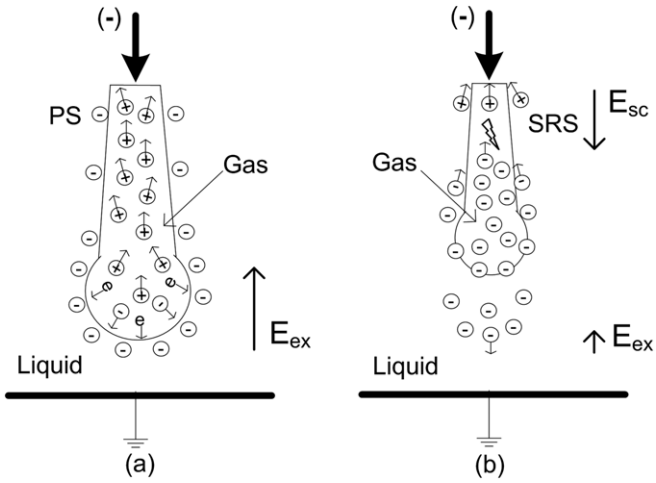

Figure 8. Schematic illustration of SRS formation, (*a*) termination of PS, (*b*) formation of SRS.

streamer images of which SRS-A has very bright channels and SRS-B is relatively weak, as compared with the PS.

All the characteristics of SRSs including polarity, length, velocity, light, shape and mode are summarized in table 1, as compared with those of the PSs. It should be emphasized that SRS is a positive polarity discharge under a negative impulse voltage, which is opposite the PS, i.e. a negative streamer under a negative voltage.

3.3. Discussion on mechanism of SRS

The possible mechanism leading to the SRS is illustrated in figure 8. Both gaseous and electronic processes are involved in the mechanism of negative streamers in liquids [22, 23], thus thermal vaporization, charge injection and local ionization could contribute to the streamer initiation and propagation. The consequence of these mechanisms is that gaseous channels filled with many charged particles are left in the liquid when the PS stops, as shown in figure 8(*a*). However the exact nature of the gaseous channels, e.g. chemical compositions, pressure and temperature, remains unclear. It should be stressed that the molecule of the Midel-7131 liquid, used in this study, contains electronegative oxygen atoms, which help in trapping the free electrons to form negative ions. So many negative ions are accumulated at the gas/liquid interface and its adjacent areas during the PS's propagation.

After the termination of PS, the external electric field E_{ex} will still be continuously expelling those negative ions at the streamer head to the ground electrode and those positive ions mainly in the streamer channels to the needle electrode, even E_{ex} decreases with the decay of applied impulse voltage; on the other hand, the gaseous channel gradually dissipates itself into the surrounding liquid. In figure 8(*b*), with further decay

Table 2. Chopping time at the tail of impulse waveform.

Voltage (kV)	$T_{PS\text{-}Stop}$ (μs)	T_{Chop} (μs)	T_{Chop}-$T_{PS\text{-}Stop}$ (μs)
60	4.63	7.26	2.63
70	11.00	15.12	4.11
80	15.94	25.37	9.44
90	12.56	25.44	12.89
100	20.40	37.71	17.31
110	24.39	37.17	12.78
120	25.14	39.09	13.96
130	31.57	37.46	5.88

of the external field, the negative ions are not necessarily moving towards the ground electrode, and they could travel back towards the needle electrode due to the process of charge diffusion. In addition, shrinkage of the streamer channel helps to bring the negative ions, those around the gas/liquid phase, back towards the needle electrode. Lastly, most of the positive ions get attached to the needle electrode. Compared with the surrounding negative charges, the needle electrode exhibits positive and therefore space charge induced electric field E_{sc} with reverse polarity is built up. Moreover, there is still a gaseous phase remaining in this area, which could offer an easier environment for the initiation of SRS. So SRS occurs eventually near the needle electrode with reverse polarity.

Initiation of SRS depends on the net field ($E_{sc} - E_{ex}$) at the needle tip. The maximum electric field E_{max} at the needle tip caused by externally applied voltage can be estimated based on Mason's equation [24],

$$E_{max} = \frac{2 \times V}{r \times \ln(1 + (4d/r))}, \quad (1)$$

where V is the applied voltage at the needle tip, r is the tip radius of the needle electrode and d is the gap distance between the needle and plane electrodes.

As seen in figure 4, the apparent inception voltage of SRS is 80 kV; however, at the time when the SRS appears, the applied impulse voltage has decayed, on average, to 12% of the peak voltage, i.e. $V = 9.6$ kV. Knowing the electrode configuration as $r = 50\,\mu$m and $d = 50$ mm, E_{ex} is calculated as 0.46 MV cm^{-1} when the SRS occurs. According to our previous shadowgraph observations, residual gaseous channels remain around the needle tip for at least a few hundred microseconds after the termination of PS, so initiation of SRS could be in either gaseous phase or liquid phase. Assuming that initiation of SRS occurs in the gaseous phase and using the corona discharge inception field of 0.03 MV cm^{-1} as a representative value of the minimum required net field, the space charge induced field E_{sc} should be 0.49 MV cm^{-1} (0.03 MV cm^{-1}+0.46 MV cm^{-1}). On the other hand, assuming the initiation of SRS occurs in the liquid phase, the net field strength needs to be 2.41 MV cm^{-1} calculated using equation (1) based on the inception voltage in figure 4 ($V = 50$ kV), therefore the space charge induced field E_{sc} should be 2.87 MV cm^{-1} (2.41 MV cm^{-1} + 0.46 MV cm^{-1}). Overall, the minimum space charge induced field to initiate an SRS would be in the range between 0.49 and 2.87 MV cm^{-1}.

In general, observation of SRS is repeatable under every shot of impulse voltage above the inception level. At the same

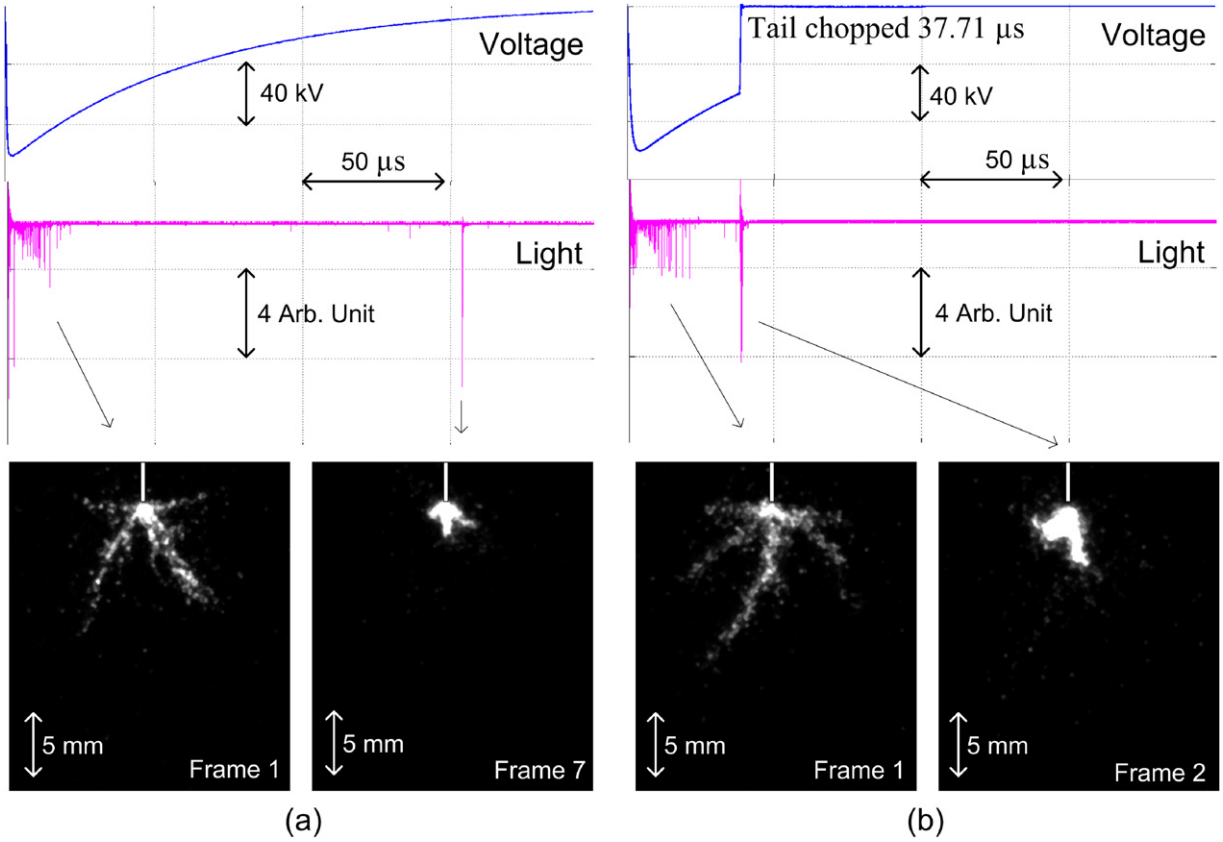

Figure 9. Effect of tail-chopped impulse on the SRS under negative impulse. $V = 100$ kV, $d = 50$ mm, (a) full waveform, 50 μs exposure time for frame 1 and 20 μs for the others, (b) tail of waveform is chopped at 37.71 μs, 30 μs exposure time for all the frames.

applied voltage, the appearance of either SRS-A or SRS-B is however random, as shown in figure 4, since the formation of SRS is determined by the internal dynamic processes, e.g. space charge generation, distribution and channel dissipation. When a strong reverse electric field is built up, SRS-A should be observed since the initiation of a 3rd mode streamer requires a high electric field. Otherwise SRS-B would be observed at a relatively weak reverse electric field. Measurement of space charge distribution may offer more evidence on the dynamic process and help to explain the type difference of SRS, so it is worthy of further investigation.

Once initiated, the SRS propagates preferably following some of the residual channels of the PS. However, there are also exceptions where new channels other than the residual ones are developed and this is especially true in the case for SRS-A.

3.4. Verification test

A remarkable feature for the occurrence of SRS is that the instantaneous voltage has to decay to a certain low level, which seems to be a necessary condition to form the SRS. Therefore in this section, the effect of tail-chopped impulse on the SRS was investigated at the same 50 mm gap under negative polarity. With the previous experiences on the propagation time of PSs, the tail of the applied impulse voltage was chopped accordingly to ensure that the voltage was there to support the full propagation of PSs but disappeared much earlier than the normal occurrence time of SRSs.

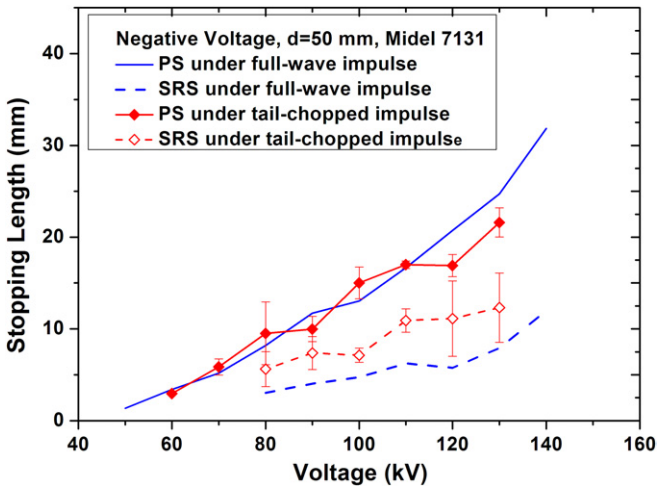

Figure 10. Stopping length of PS and SRS under full-wave and tail-chopped impulse voltages.

The detailed chopping time at each applied voltage level is given in table 2. Variance of time interval $T_{\text{Chop}} - T_{\text{PS-Stop}}$ inevitably occurred in the range 10 ± 8 μs and this is mainly for two reasons: firstly, the limitation of the chopping device to control the exactly desired chopping time T_{Chop} of an impulse shot at high voltage levels; and secondly, the natural scattering of the stopping time of a primary streamer $T_{\text{PS-Stop}}$. Nevertheless, this verification test still serves the purpose of validating the mechanism proposed in section 3.3 by removing

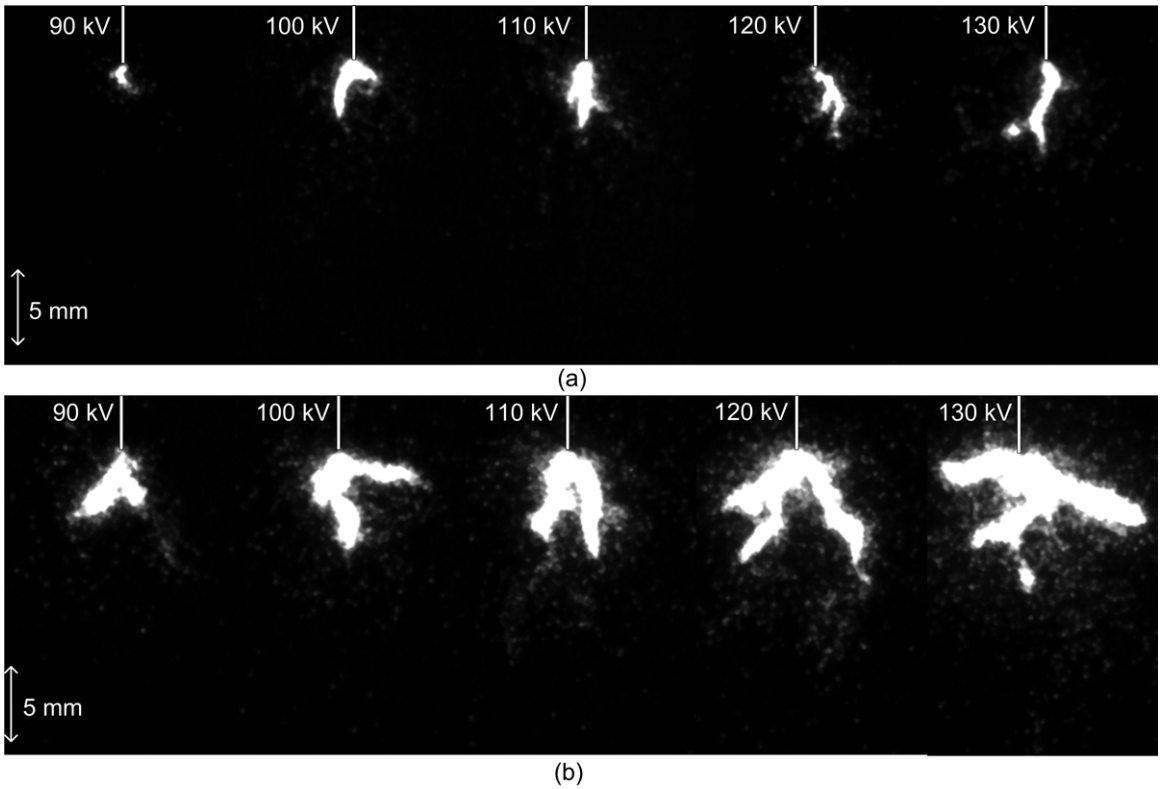

Figure 11. Images of SRS under negative full-wave and tail-chopped impulse voltages, (*a*) SRS under full-wave impulse, (*b*) SRS under tail-chopped impulse.

the externally applied E_{ex} and leaving the internally formed E_{sc} as the only responsible parameter for SRS, despite the variance of the time interval $T_{Chop} - T_{PS\text{-}Stop}$.

Figure 9 shows an example to demonstrate the effect of tail-chopped impulse on the SRS, obtained under negative 100 kV impulse voltages. As shown in figure 9(*a*) under full-wave impulse voltage, a normal SRS-A with a length of 3.49 mm was observed at 153.78 μs, well after the termination of PS. The length of the PS is 11.17 mm. In figure 9(*b*), the tail of impulse was chopped at 37.71 μs after the full propagation of PS which stopped at 19.75 μs with a length of 13.78 mm. It was found that the occurrence of SRS was advanced in time, occurring just after the impulse was chopped. Therefore the time of occurrence of SRS under tail-chopped impulse was the same as the corresponding chopping time. Afterwards, there was nothing observed either in light signal or in still images. Unfortunately, the light signal of SRS is overlapped with the discharging noise induced by the chopping wave; however, it is evidenced in still image frame 2 that SRS with a length of 6.58 mm does occur and has very bright thick channels resembling the features of SRS-A under the full-wave impulse.

Figure 10 shows the stopping length of both PSs and SRSs under full-wave and tail-chopped impulse voltages. Since the impulse was chopped after the full propagation of PSs as indicated in table 2, it is understandable to see that the stopping lengths of PSs under tail-chopped impulse voltages are similar to those under full-wave impulse voltages. However, SRSs are not only advanced in time, but also promoted in length by the tail-chopped impulses. As seen in figure 10, the stopping lengths of SRSs under tail-chopped impulse voltages are generally larger than those under full-wave impulse voltages.

The shape features of SRS under tail-chopped impulse voltages are shown in figure 11. Since SRSs under tail-chopped impulse resemble the features of SRS-As under full-wave impulse, the still images of SRSs under tail-chopped impulses are compared with those of SRS-As under full-wave impulses. It is striking that SRSs under tail-chopped impulses have more branches and much thicker channels than SRS-As under full-wave impulses, especially at higher voltage levels. In addition, the multi-branch shape of SRS radiating from the needle point as shown in figure 11(*b*) supports the assumption that the SRS is most likely to be developed in the direction from the needle point to the surrounding liquid. However, this should be confirmed using fast imaging observation in a future study.

As illustrated in section 3.3, space charge plays an important role in building up the reverse electric field E_{sc} to compete with the external field E_{ex} produced by the full wave impulse voltage. Hence there has to be a certain time of delay for the external field decaying to a low level so that the net field ($E_{sc} - E_{ex}$) can reach the inception threshold of SRS. The full-wave experiments so far show that this could take approximately 142.57 μs on average; during this period, some of the residual charges are indeed lost into the cathode or anode or through recombination.

Chopping at the tail of impulse after the full propagation of PS firstly makes sure that space charges are generated by the PS and secondly removes the effect of the external field completely and instantaneously, i.e. $E_{ex} = 0$. Therefore,

the net field ($E_{sc} - E_{ex}$) under tail-chopped impulse is much higher than the case under the full-wave impulse when E_{ex} is non-zero, and thus the SRSs occur immediately after the tail chopping and are much stronger than those under full-wave impulse. Consequently, tests under tail-chopped impulse further confirm the important role of space charges in the formation of SRS.

4. Conclusion

Two types of SRS were observed in an ester insulating liquid under negative 1.2/50 μs impulse voltage. In the investigated range from 40 to 140 kV, the PS resembles the features of 2nd mode streamer while the two types of SRS, SRS-A and SRS-B, belong to 3rd mode and 2nd mode, respectively. In terms of stopping length, both types of SRS are comparable and they are shorter than the PSs. Generally both types of SRS occur on average at the time of 142.57 μs, when the instantaneous voltage has decayed to approximately 12% of the peak value of impulse.

It should be stressed that SRS under negative impulse voltages has positive polarity, which is opposite the PS. Therefore space charge induced reverse electric field is the key mechanism of SRS. To sum up, the formation of SRS probably needs the following three conditions: (1) a decayed impulse waveform, (2) sufficient residual space charges and (3) a favourable gaseous environment. In addition, the liquid nature, e.g. electronegative performance and viscosity, might also have a considerable effect on the formation of SRS, which is worthy of further study.

Acknowledgments

The authors would like to express their gratitude to ALSTOM Grid, M&I Materials, National Grid, Scottish Power, TJ|H2b Analytical Services and UK Power Networks for their financial and technical support. Sincere thanks are given to EPSRC Instrument Pool for the loan of the high-speed camera.

References

[1] Hudson G G and Loeb L B 1961 Streamer mechanism and main stroke in the filamentary spark breakdown in air as revealed by photomultipliers and fast oscilloscopic techniques *Phys. Rev.* **123** 29

[2] Hebner R E 1988 *The Liquid State and its Electrical Properties* (New York: Plenum) p 519

[3] Lesaint O 2008 'Streamers' in liquids: relation with practical high voltage insulation and testing of liquids *IEEE Int. Conf. on Dielectric Liquids (ICDL) (Poitiers, France)* p 120

[4] Lesaint O and Top T V 2002 Streamer initiation in mineral oil. Part I: electrode surface effect under impulse voltage *IEEE Trans. Dielectr. Electr. Insul.* **9** 84

[5] Sharbaugh A H, Devins J C and Rzad S J 1978 Progress in the field of electric breakdown in dielectric liquids *IEEE Trans. Electr. Insul.* **EI-13** 249

[6] Yamashita H, Amano H and Mori T 1977 Optical observation of pre-breakdown and breakdown phenomena in transformer oil *J. phys. D: Appl. phys.* **10** 1753

[7] Forster E O 1985 Critical assessment of the electrical breakdown process in dielectric fluids *IEEE Trans. Electr. Insul.* **EI-20** 891

[8] Beroual A and Tobazeon R 1986 Prebreakdown phenomena in liquid dielectrics *IEEE Trans. Electr. Insul.* **EI-21** 613

[9] Watson P K, Chadband W G and Sadeghzadeh-Araghi M 1991 The role of electrostatic and hydrodynamic forces in the negative-point breakdown of liquid dielectrics *IEEE Trans. Electr. Insul.* **26** 543

[10] Linhjell D, Lundgaard L and Berg G 1994 Streamer propagation under impulse voltage in long point-plane oil gaps Dielectrics and Electrical Insulation *IEEE Trans. Dielectr. Electr. Insul.* **1** 447

[11] O'Sullivan F, Hwang J G, Zahn M, Hjortstam O, Pettersson L, Rongsheng L and Biller P 2008 A Model for the initiation and propagation of positive streamers in transformer oil *IEEE Int. Symp. on Electr. Insul. (ISEI) (Vancouver)* p 210

[12] Torshin Y V 2009 Initiation and propagation of the negative leader in transformer oil under impulse voltage *IEEE Trans. Dielectr. Electr. Insul.* **16** 1536

[13] Beroual A, Zahn M, Badent A, Kist K, Schwabe A J, Yamashita H, Yamazawa K, Danikas M, Chadband W D and Torshin Y 1998 Propagation and structure of streamers in liquid dielectrics *IEEE Electr. Insul. Mag.* **14** 6

[14] Kolb J F, Joshi R P, Xiao S and Schoenbach K H 2008 Streamers in water and other dielectric liquids *J. Phys. D: Appl. phys.* **41** 234007

[15] Shimazaki T 1992 Flashover characteristics and surface processes under negative impulse voltage in atmospheric air *IEEE Trans. Electr. Insul.* **27** 488

[16] Murooka Y and Koyama S 1973 Nanosecond surface discharge study by using dust figure techniques *J. Appl. Phys.* **44** 1576

[17] Kebbabi L and Beroual A 2006 Optical and electrical characterization of creeping discharges over solid/liquid interfaces under lightning impulse voltage *IEEE Trans. Dielectr. Electr. Insul.* **13** 565

[18] Liu Q and Wang Z D 2011 Streamer characteristic and breakdown in synthetic and natural ester transformer liquids under standard lightning impulse voltage *IEEE Trans. Dielectr. Electr. Insul.* **18** 285

[19] Lesaint O and Massala G 1998 Positive streamer propagation in large oil gaps: experimental characterization of propagation modes *IEEE Trans. Dielectr. Electr. Insul.* **5** 360

[20] Lundgaard L, Linhjell D, Berg G and Sigmond S 1998 Propagation of positive and negative streamers in oil with and without pressboard interfaces *IEEE Trans. Dielectr. Electr. Insul.* **5** 388

[21] Duy C T, Lesaint O, Denat A and Bonifaci N 2009 Streamer propagation and breakdown in natural ester at high voltage *IEEE Trans. Dielectr. Electr. Insul.* **16** 1582

[22] Beroual A 1993 Electronic and gaseous processes in the prebreakdown phenomena of dielectric liquids *J. Appl. Phys.* **73** 4528

[23] Massala G and Lesaint O 2001 A comparison of negative and positive streamers in mineral oil at large gaps *J. Phys. D: Appl. phys.* **34** 1525

[24] Mason J H 1955 Breakdown of solid dielectrics in divergent fields *Proc. IEE C: Monogr.* **102** 254